Why does the jumping ciliate *Mesodinium rubrum* possess equatorially located propulsive ciliary belt?

Houshuo Jiang

Department of Applied Ocean Physics and Engineering, Woods Hole Oceanographic Institution, Woods Hole, Massachusetts 02543, USA

E-mail: hsjiang@whoi.edu

(Submitted to *Journal of Plankton Research* on December 3, 2010)
(Revision submitted to *Journal of Plankton Research* on January 14, 2011)
(Accepted for publication in *Journal of Plankton Research* on January 16, 2011)

ABSTRACT

It has long been thought that jumping by the ciliate *Mesodinium rubrum* can enhance its nutrient uptake. However, jumping can be energetically costly and also dangerous by inducing hydrodynamic disturbances detectable to rheotactic predators. Here, a computational fluid dynamics (CFD) model, driven by published empirical data, is developed to simulate the jump-induced unsteady flow as well as chemical field around a self-propelled jumping ciliate. The associated phosphorus uptake, hydrodynamic signal strength, mechanical energy cost and Froude propulsion efficiency are also calculated. An equatorial ciliary belt (ECB), i.e. the morphology used by *M. rubrum* for propulsion, is considered. For comparison purpose, three other strategies (pulled or pushed by cilia, or towed) are also considered. Comparison of the CFD results among the four strategies considered suggests: (1) jumping enhances phosphorus uptake with simulated values consistent with available field data; (2) the *M. rubrum*-like propulsion generates the weakest and spatially most limited hydrodynamic disturbance and therefore may effectively minimize the jump-induced predation risk; and (3) the *M. rubrum*-like propulsion achieves a high Froude propulsion efficiency (~0.78) and is least costly in mechanical energy expenditure among the three self-propelled strategies considered. Thus, using the ECB for propulsion can be essential in ensuring that *M. rubrum* is a successful 'fast-jumping' primary producer.

Keywords: jumping ciliate, *Mesodinium rubrum*, nutrient uptake, hydrodynamic signal, Froude propulsion efficiency, computational fluid dynamics

INTRODUCTION

The ubiquitous marine planktonic ciliate *Mesodinium rubrum* Lohman (*Myrionecta rubra* Jankowsky) is probably one of the most remarkable among those red-water organisms in that it is a fast-jumping primary producer (Lindhohm, 1985). The body shape of *M. rubrum* consists roughly of a hemispherical oral end and a conical aboral end (e.g. Taylor et al., 1971; Lindhohm, 1985; Fenchel and Hansen, 2006), with the overall body size ranging ~15-70 μm (Lindhohm, 1985). The external morphology also includes some bifurcated oral tentacles, an equatorial girdle of cirri and a dense equatorial ciliary belt (ECB) that forms a skirt extending halfway toward the aboral end (Fig. 1). Probably ever since Darwin, it has been known that this ciliate species jumps at an extraordinary speed (Darwin, 1839; Taylor et al., 1971; Lindhohm, 1985). However, the details of the rapid jumping movements have only been revealed very recently by using 1000-frame-per-second high-speed video recording (Fenchel and Hansen, 2006). An individual *M. rubrum* (~23 μm in body size) has been shown to reach a maximum body speed of ~11 mm s^{-1} and to cover a jumping distance ~160 μm, with the aboral end forwards (Fig. 1), all within a single beat (lasting ~20 ms) of the membranelles that form from the cilia of the ECB. This can by no means be matched by any other phytoplankton species that are equipped with different propulsive morphologies (see below). Nevertheless, *M. rubrum* can achieve unusually high photosynthetic rates and be a major primary producer in coastal ecosystems (e.g. Packard et al., 1978; Smith and Barber, 1979; Crawford, 1989; Stoecker et al., 1991; Stoecker et al., 2009).

The adaptive significance of fast jumping in *Mesodinium rubrum* has been recently summarized (Fenchel and Hansen, 2006; Riisgård and Larsen, 2009). First, the rapid jumping motion enables the ciliate to escape from danger (such as in the vicinity of a copepod feeding current) and reduce the probability of being captured (e.g. Jonsson and Tiselius, 1990); such escape jumps are apparently reasonable responses when the ciliate perceives the predator-generated hydrodynamic signals (Jakobsen, 2001). Second, fast jumping can enhance nutrient uptake that may be a limiting factor for photosynthesis in *M. rubrum*. Nutrient uptake in larger immobile phytoplankton cells can be diffusion-limited (e.g. Munk and Riley, 1952; Kiørboe, 1993; Karp-Boss et al., 1996). Jumping creates fluid motion surrounding the ciliate that steepens the nutrient gradient to increase the contribution of advective transport to nutrient uptake. Third (the often upward-oriented) jumping helps *M. rubrum* to maintain itself in the euphotic zone as well as to survive the more turbulent conditions within the

upwelling waters (e.g. Margalef et al., 1979; Wilkerson and Grunseich, 1990). Importantly, it also has been shown that *M. rubrum* does not jump when it actively uses its bifurcated oral tentacles to capture prey (Yih et al., 2004), suggesting that jumping is for purposes other than prey capture.

Using the equatorial ciliary belt (ECB) for propulsion seems to be essential for *Mesodinium rubrum* to achieve the unparalleled jumping speed. This can be seen by comparing with those planktonic protists that employ other types of propulsive morphologies (e.g. Fenchel, 1987; Sleigh, 1989; Hausmann et al., 2003). Flagellates (1-50 μm in diameter) having one or more flagella on the anterior (posterior) that pull (push) swim at a low to small fraction of 1 mm s^{-1}. Dinoflagellates (10-150 μm in diameter) possess two flagella: one is a smooth, longitudinal, trailing flagellum, and the other is a hairy one situated in a groove along the equator of the cell, i.e. a transversal flagellum. Although the relative contributions of these two flagella to thrust and to overall motion of the cell are complex (Gaines and Taylor, 1985; Fenchel, 2001; Miyasaka et al., 2004), the swimming speed they achieve is ~10 body lengths s^{-1} (i.e. 0.01-1.5 mm s^{-1}). Those planktonic ciliates that are pulled (pushed) by their anterior (posterior) ciliary band swim at a speed usually in the range of 0.5 up to a few mm s^{-1}.

Often, a specific behavioral or morphological strategy can be beneficial in one aspect but detrimental in another (e.g. Tiselius et al., 1997; Visser et al., 2009). Fast jumping apparently brings several benefits as summarized before, but it may potentially generate stronger hydrodynamic disturbances that may be more easily detectable by rheotactic predators and therefore increase predation risk. It also may be accompanied by higher energy costs. Thus, we may hypothesize that the specific propulsive morphology (i.e. the ECB) that *M. rubrum* uses for fast jumping generates weaker hydrodynamic disturbances and costs less mechanical energy than if other representative propulsive morphologies were used to achieve the same fast jumping.

The focus of this study is to shed light on the strategy of using the ECB for fast jumping in *Mesodinium rubrum* by using a computational fluid dynamics (CFD) model. The CFD model computes the unsteady flow field imposed by a self-propelled jumping protist and considers several representative propulsive morphologies, including the ECB. Simultaneously, the model also computes the unsteady chemical field surrounding the jumping protist to determine nutrient uptake. The mechanical energy cost and Froude propulsion efficiency can also be calculated. These results will be compared among all considered propulsive morphologies. There are previous works on modeling the flow field (e.g. Blake, 1971; Blake, 1973; Brennen, 1974; Keller and Wu, 1977; Higdon, 1979a;

Higdon, 1979b) as well as enhancement of nutrient uptake (e.g. Magar et al., 2003; Magar and Pedley, 2005; Langlois et al., 2009; Bearon and Magar, 2010) associated with a self-propelled swimming microorganism. However, the effects due to different propulsive morphologies have seldom been investigated or compared. It is of great interest to study the advantages/disadvantages those morphological differences can bring to protists in terms of hydrodynamic conspicuousness, energetics, and material transport towards or away from the protistan body.

METHOD

Observed jump kinematics of *Mesodinium rubrum*

Using 1000-frame-per-second high-speed imaging, Fenchel and Hansen (2006) obtained a typical jump kinematics (Fig. 2) for a *Mesodinium rubrum* ciliate (~23 μm in body size). A fit to their observed time-dependent jump velocity data (Fig. 2b) was used in this study to drive the CFD modeling. The Reynolds number calculated for this jump is ~0.2, based on the body size and the maximum jump speed.

CFD simulation approach

The jumping ciliate was modeled as a sphere of radius a (= 11.5 μm) covered with a ciliary layer of thickness l (= 5.75 μm). This thickness was estimated from the generalized external morphology as shown in Fig. 1. The model ciliate is assumed to jump forward along a straight line (i.e. the x-axis; Fig. 3). As the modeled flow is axisymmetric, only a meridian plane needs to be included as the computational domain (i.e. the finite geometric domain on which the flow field is solved numerically). A cylindrical polar coordinate system is adopted with r being the radial distance from the x-axis (Fig. 3). Symmetry boundary condition is specified on the upper boundary. Pressure-outlet boundary conditions are specified on both the left and right boundary.

The computational domain is $100a$ in the x-direction and $50a$ in the r-direction (Fig. 3a). The domain is discretized into 750 quadrilateral control volumes (CVs) immediately adjacent to the spherical ciliate body and into ~24,000 triangular CVs that are stretched radially outward from the outer boundary of the quadrilateral CVs. The model-ciliate body and the quadrilateral CVs travel together (Fig. 3) according to the observed time-dependent jump velocity, $U(t)$. The outer zone

consisting of the triangular CVs (i.e. the deforming mesh zone; Fig. 3b) is remeshed every time step in order to accommodate the combined motion of the model-ciliate body (as an internal solid-wall boundary) and the adjacent quadrilateral CV zone.

There is no relative motion between the model-ciliate body and the adjacent quadrilateral CV zone, and the quadrilateral CV zone remains un-deformed throughout the jump duration. It is therefore feasible to apply on the quadrilateral CV zone a spatially consistent time-dependent field of body force, $\mathbf{F}(x, r, t$; in N m^{-3}), to model the forcing due to beating of the cilia. Via such a CFD setup, the forcing and the model-ciliate body translate together, which is analogical to the real world situation that the beating cilia translate with the ciliate body. The axial, $F_x(x, r, t)$, and radial, $F_r(x, r, t)$, component of the forcing are specified as:

$$F_x(x,r,t) = -f(t)\sin(\pi\eta)\frac{r'}{\sqrt{x'^2 + r'^2}} \tag{1a}$$

$$F_r(x,r,t) = f(t)\sin(\pi\eta)\frac{x'}{\sqrt{x'^2 + r'^2}} \tag{1b}$$

where $\eta = \dfrac{\sqrt{x'^2 + r'^2} - a}{l}$ with a the radius of the model ciliate and l the thickness of the ciliary layer as defined above. $r' = r$ and $x' = x - x_{\text{ciliate}}(t)$, where $x_{\text{ciliate}}(t)$ is the model ciliate's instantaneous axial position that is determined from the observed time-dependent jump velocity, $U(t)$. $f(t)$ is the time-dependent forcing density (in N m^{-3}), which needs to be determined at every time step (see below). Such a specification of the forcing is based on an analytical solution for an infinite, plane ciliary layer (Wu, 1977). The solution provides the optimum distribution of the average ciliary continuum force under the condition of minimum power required for fixed mean square force.

Four ciliary forcing schemes were considered in this study, with the real-world ciliary propulsive morphologies in mind: (i) the equatorial surface of the model ciliate is covered by cilia, with **F** being non-zero only in the polar angle range from 72 to 108° (Fig. 4a); (ii) the anterior surface of the model ciliate is covered by cilia, with **F** being non-zero only in the polar angle range from 0 to 36° (Fig. 4b); (iii) the posterior surface of the model ciliate is covered by cilia, with **F** being non-zero only in the polar angle range from 144 to 180° (Fig. 4c); and (iv) **F** is zero throughout the ciliary layer with the model ciliate being towed forward (Fig. 4d).

The flow field associated with a jumping ciliate can be taken as laminar, incompressible and Newtonian, and is governed by the unsteady incompressible Navier-Stokes equations together with the continuity equation (not shown for brevity). To obtain the flow field, these equations under the above-described forcing and boundary conditions were numerically solved by using the commercially available finite-volume CFD software package ANSYS FLUENT (version 12.0.16; Lebanon, New Hampshire, USA). Using a stationary frame of reference, the model-ciliate body motion, $U(t)$, is explicitly included as a prescribed moving solid-wall boundary condition. To ensure that $U(t)$ is a result of self-propulsion by the model ciliate, the ciliary forcing $\mathbf{F}(x, r, t)$ is determined at every time step by solving the dynamic equation of the model-ciliate jump:

$$m_{\text{ciliate}} \frac{dU(t)}{dt} = R(t) + T(t) \tag{2}$$

where m_{ciliate} is the body mass of the model ciliate. $R(t)$ is the instantaneous hydrodynamic resistance (with the added mass effect included) acting on the body surface of the model ciliate and $T(t)$ is the instantaneous thrust. $R(t)$ is obtained by determining the axial component of the area integral of pressure and shear stress over the body surface. $T(t)$ is equal to the axial component of the volume integral of $\mathbf{F}(x, r, t)$ over the volume where the ciliary forcing is applied. Because the general form of $\mathbf{F}(x, r, t)$ is prescribed by Equation (1), Equation (2) is solved by determining the coefficient, $f(t)$, in front of the prescribed general form. In practice, at each time step $\mathbf{F}$ is first determined on the basis of the flow field information at the immediately previous time step, and then the determined $\mathbf{F}$ is coupled to the flow field solver, along with the moving/deforming mesh, to compute the flow field at the next time step. Thus, a small time step is necessary for both accuracy and convergence (see below). For more details on the solution process, interested readers are referred to User's Guide of ANSYS FLUENT.

The chemical field, $C(x, r, t)$, around the jumping ciliate can be described by the advection-diffusion equation:

$$\frac{\partial C}{\partial t} + \mathbf{u} \cdot \nabla C = D \nabla^2 C \tag{3}$$

where $\mathbf{u}$ is the jump-imposed flow field and D is a constant diffusivity (diffusion coefficient). Simultaneously to the solution of the flow equations, Equation (3) was solved by using ANSYS FLUENT and subject to the boundary conditions:

$C = 0$, at the surface of the ciliate (4a)

$C \to C_\infty$ (a constant), at infinity (4b)

and the initial condition:

$$C(x, r, t = 0) = C_\infty \left(1 - \frac{a}{\sqrt{(x - x_0)^2 + r^2}} \right) \quad (5)$$

where x_0 is the initial axial position of the model ciliate. Here, the boundary condition applied at the surface of the ciliate is the Dirichlet boundary condition, which is suitable for considering how propulsion enhances the diffusion-limited nutrient uptake by the ciliate (e.g. Bearon and Magar, 2010). The initial condition used is simply the steady-state (i.e. $\frac{\partial C}{\partial t} = 0$) and diffusion-only ($\mathbf{u} = 0$) solution of Equation (3).

Throughout this study, the fluid density, ρ, is 1.02695×10^3 kg m^{-3} and the fluid kinematic viscosity, ν, is 1.354×10^{-6} m^2 s^{-1}; both are the values for seawater with salinity 35 at 10°C at one normal atmosphere. The mass density of the model ciliate is assumed to be equal to the fluid density. The chemical diffusivity, D, is 1.0×10^{-9} m^2 s^{-1} (e.g. for phosphorus uptake).

As to the numerical schemes, the highly accurate third-order MUSCL (monotone upstream-centered schemes for conservation laws) scheme is used for spatial interpolation. The body force weighted scheme is selected as the discretization method for pressure. The PISO (pressure-implicit with splitting of operators) scheme is used for pressure-velocity coupling. Temporal discretization is a first-order implicit scheme. For the jumping phase, the time step is $t^*/100$ where $t^* = a^2/\nu$ (~ 97.7 ms; a viscous time scale based on the radius of the model ciliate). Using such a small time step is also a requirement by the dynamic (moving/deforming) mesh model in ANSYS FLUENT. At the end of the jumping phase, when the model ciliate is almost stationary, the dynamic mesh model is switched off to allow for a much larger time step (= t^*). After the jumping phase, the simulation is still continued for a significantly long time, e.g. 150,000 × t^* (~14.7 s). As a result, the time-dependent flow field as well as chemical field is also obtained for the decay phase. The choices of these time steps and of the mesh sizes described previously are based on a series of mesh and time-step refinement studies (not shown for brevity). Validation of the CFD code performance is presented in the Appendix.

Volume of influence of the jump-imposed flow

Rheotactic predators are likely to respond to the velocity magnitude of the flow imposed by moving prey (Kiørboe and Visser, 1999). Here, the jumping ciliate is considered a moving prey; the volume of influence of the ciliate-imposed flow is defined as the volume within which the instantaneous flow velocity exceeds a threshold magnitude, u^*. The time series of volume of influence, $V(t)$, is obtained for every time step from the simulated time-dependent jumping flow field for each of the four ciliary forcing schemes considered.

Thrust, power and propulsion efficiency

During the power stroke, the instantaneous thrust, $T(t)$, is obtained at every time step by solving Equation (2) and the flow field equations jointly as described previously. The instantaneous mechanical power, $P(t)$, applied by the cilia is calculated as the volume integral of $[\mathbf{F}(x, r, t)\cdot\mathbf{u}(x, r, t)]$ over the volume where the ciliary forcing, $\mathbf{F}(x, r, t)$, is applied; here $\mathbf{u}(x, r, t)$ is the CFD-simulated instantaneous flow velocity vector field. The CFD-simulated total mechanical work, W_{CFD}, is then calculated as the time integral of $P(t)$ over the power stroke duration, τ.

The hydromechanical efficiency (or Froude propulsion efficiency; Lighthill, 1970) for ciliate jumping is calculated according to its definition:

$$\xi = \frac{\int_0^{\tau} T(t)U(t)\,dt}{W_{\mathrm{CFD}}} \tag{6}$$

where the useful mechanical work is calculated as the time integral of the product of the instantaneous thrust, $T(t)$, and jump velocity, $U(t)$, over the power stroke duration, τ.

Nutrient uptake

From the simulated chemical field, $C(x, r, t)$, around the jumping ciliate, the total flux of the chemical (or nutrient) to the ciliate is calculated at every time step as (e.g. Karp-Boss et al., 1996):

$$J = -D\iint_S \mathbf{n}\cdot\nabla C\,dS \tag{7}$$

where S is the ciliate surface and **n** is the unit normal inward to S. The Sherwood number, Sh, is also calculated at every time step from its definition:

$$\mathrm{Sh} \equiv J/J_D \tag{8}$$

where $J_D = 4\pi aDC_\infty$, which is the flux due to diffusion only. Thus, Sh quantifies the relative enhancement of flux due to advection caused by the jump-imposed flow.

RESULTS

The jump-imposed hydrodynamic disturbance

Both the flow pattern and the spatial decay of the hydrodynamic disturbance created by a jumping model-ciliate are sensitive to the way the ciliate propels itself; both vary greatly for the four ciliary forcing schemes considered in this study (Fig. 5). In the case where the equatorial surface of the model ciliate is covered by cilia (i.e. the *Mesodinium rubrum*-like propulsion), the flow pattern is not stresslet-like (i.e. two oppositely directed jet-like flows extending both in front of and behind the ciliate) and the imposed flow velocity (relative to a stationary frame of reference) around the ciliate is always less than the instantaneous jumping velocity of the ciliate (Fig. 5a); the instantaneous flow attenuates with distance, d, as $\sim d^{-3}$ (not shown), which is similar to what has been previously shown for steady swimming via equatorially distributed cilia (Jiang and Paffenhöfer, 2008). In cases where the ciliate is either pulled (Fig. 5b) or pushed (Fig. 5c) by the cilia, the flow patterns are stresslet-like and velocities both within and surrounding the ciliary-forcing region are much greater than the instantaneous jumping velocity of the ciliate; these two flow fields have similar spatial decay rates ($\sim d^{-2}$) but are opposite in flow directions. In the towed-body case, the flow is of a Stokeslet-like flow pattern (Fig. 5d) and decays much slower spatially ($\sim d^{-1}$).

The time series of volume of influence calculated, respectively, for the four imposed hydrodynamic disturbances are shown in Fig. 6. The forcing scheme of equatorially distributed cilia (i.e. the *Mesodinium rubrum*-like propulsion) generates a disturbance with the smallest spatial extension; the towed body generates the largest, while both the puller and the pusher generate disturbances with spatial extension lying in between. The differences in volume of influence among these imposed hydrodynamic disturbances are enormous.

Thrust, power and Froude propulsion efficiency

The CFD-simulated thrust, power and Froude propulsion efficiency for jumping are all different among the four ciliary forcing schemes considered in this study (Fig. 7; Table 1). Although differing slightly among themselves, the three self-propelled ciliary forcing schemes require much higher thrust than the force required to tow the body (Fig. 7b). In terms of mechanical power input, the towed body of course requires the lowest level; the forcing scheme of equatorially distributed cilia (i.e. the *Mesodinium rubrum*-like propulsion) requires ~3.5 times higher mechanical power input than that for towing the body, while both the puller and the pusher require even much higher levels of mechanical power input (Fig. 7c). The *M. rubrum*-like propulsion achieves a much higher Froude propulsion efficiency (~0.775) than both the puller (~0.126) and the pusher (~0.139) do (Table 1); the Froude propulsion efficiency for the trivial case of the towed body is 1. For all cases considered, mechanical energy expenditure, averaged over a long time period, is only a small percentage of the total metabolic rate (5th column in Table 1).

Chemical field, Sherwood number and nutrient uptake

The three self-propelled ciliary forcing schemes generate much sharper chemical gradients near the ciliate surface than the towed-body model does (Fig. 8). The three self-propelled models also generate a local concentration minimum near the starting position of the jump (Fig. 8a, b, c), which is, however, not present in the towed-body model (Fig. 8d). For phosphorus uptake ($D = 1.0\times10^{-9}$ m^2 s^{-1}), the three self-propelled models achieve a maximum Sherwood number ~5, in contrast to ~3 reached by the towed-body model (Fig. 9). Among the three self-propelled models, the puller achieves the highest uptake, the *Mesodinium rubrum*-like propulsion follows and the pusher achieves the lowest uptake, though the three models differ not too much from each other (Fig. 9). Importantly, the often-used theoretical solution for the steady-state situation reproduces none of these CFD-simulated jumping cases, either self-propelled or towed (Fig. 9).

Although it takes only a very short time for the ciliate to build up the sharp chemical gradients surrounding its body surface via jumping (t = 0.0, 0.0093, 0.0186 s in Fig. 10), after the jump is completed it takes seconds for the chemical field with sharp gradients to relax to its pre-jump

configuration (t = 0.1016, 1.0005, 10.0004 s in Fig. 10). Thus, significant nutrient uptake can be achieved during the couple of seconds immediately following the jump (Fig. 11, with details presented in DISCUSSION).

DISCUSSION

Jumping and nutrient uptake

Field data available in the literature allows for a rough estimate of phosphorus-uptake rates by *Mesodinium rubrum* (~40 μm in cell diameter) in bloom water in the Baja California upwelling system (Station 73, Packard et al., 1978). At this station, *M. rubrum* photosynthetic rate was measured to be 468 μg C hr^{-1} L^{-1}. For the surface water, two different cell counts were obtained, i.e. 7.1×10^{4} cells L^{-1} (large Niskin bottle sample) versus 5.38×10^{5} cells L^{-1} (bucket sample). Based on the Redfield ratio C:P = 106:1 (Redfield, 1958), one can work out two phosphorus-uptake rates, i.e. 2.9×10^{-19} mol P μm^{-2} s^{-1} for the lower cell counts and 0.38×10^{-19} mol P μm^{-2} s^{-1} for the higher cell counts, both expressed as the cell surface area-specific flux. The former value falls within the range of the maximum phosphorus-uptake rates of phytoplankton (0.5×10^{-19}-35×10^{-19} mol P μm^{-2} s^{-1}; Reynolds, 2006). In the surface water of the same station, PO_4^{3-} concentration was ~1.43 μmol L^{-1}, whereas at stations where *M. rubrum* did not occur the average concentration was 0.6 μmol L^{-1}. Note that the external concentrations required to saturate the rates of growth of phytoplankton are generally under 0.13 μmol L^{-1} (Reynolds, 2006). From the CFD-simulated chemical field and using Equation (7), the instantaneous phosphorus-uptake rate, J, was calculated, respectively, for the 3 levels of external background phosphorus concentration (C_∞ = 0.13, 0.6, 1.43 μmol L^{-1}) and the results are shown in Fig. 11. For the lowest concentration, the calculated phosphorus-uptake rate is mostly below the minimum requirement for the bloom uptake rate estimated from the field data; while for the two higher concentrations, the calculated rates are within the requirement range. In each of these three calculation examples, jumping generates a peak in the uptake rate, and the post-jump time period contributes substantially more to the overall uptake than the jumping time period. These observations support the view that jumping by *M. rubrum* can significantly enhance its nutrient uptake.

Previous behavioral observation shows that *Mesodinium rubrum* jumps approximately every 1-10 s (e.g. Fenchel and Hansen, 2006). The observed time interval between jumps is significantly larger

than the diffusion time scale based on the ciliate body radius (i.e. $a^2/D = 0.132$ s, for $a = 11.5$ μm and $D = 1.0\times10^{-9}$ m^2 s^{-1}) but close to the diffusion time scale based on half jumping distance (i.e. $(L_{max}/2)^2/D = 6.4$ s, for $L_{max} = 160$ μm and $D = 1.0\times10^{-9}$ m^2 s^{-1}). This suggests that those jumps repeated at the observed time intervals may be for rebuilding the chemical field with sharp gradients before it completely relaxes to the chemical field resulting from pure diffusion.

The theoretical solution for the steady state situation has been shown to be unable to reproduce any of the CFD-simulated results for ciliate jumping (Fig. 9). Ciliate jumping is highly unsteady and characterized by a jumping time much shorter than the diffusion time scale. Thus, in order to more accurately calculate the associated nutrient uptake, using transient CFD simulations such as those presented in this study seems necessary. Researchers have previously pointed out the importance of finding the unsteady solution to the advection-diffusion equation governing a time-dependent chemical field (e.g. Bearon and Magar, 2010; Strom and Fredrickson, 2010).

Benefits from adopting the equatorial distribution of cilia

Fast jumping has been shown probably to benefit the ciliate *Mesodinium rubrum* by enhancing its nutrient uptake. However, jumping may require higher mechanical power input and may also expose the ciliate to rheotactic predators by generating elevated hydrodynamic disturbances. The present numerical study reveals the probable advantages of adopting equatorially distributed cilia in the *M. rubrum*-like propulsion over two other propulsion strategies (i.e. pulled or pushed by cilia). The *M. rubrum*-like propulsion generates a much weaker and spatially much more limited hydrodynamic disturbance and therefore may effectively minimize the jump-induced predation risk from rheotactic predators. Also, the *M. rubrum*-like propulsion requires much less mechanical power input and simultaneously achieves a much higher Froude propulsion efficiency. All these advantages stem from the fact that the *M. rubrum*-like propulsion imposes a jumping flow with spatial pattern and attenuation very different from those imposed by the other two propulsion strategies (see RESULTS). In particular, the reason for the much lower mechanical energy costs in the *M. rubrum*-like propulsion is that in it the equatorially distributed cilia push against the flow of magnitudes always smaller than the instantaneous jumping velocity; while in the other two strategies, the magnitudes of the flow that the cilia push against are always larger than the instantaneous jumping velocity. Thus, the equatorial distribution of

propulsive cilia (the ECB) can be essential for *M. rubrum* to be an ecologically successful 'fast-jumping' primary producer.

In the *Mesodinium rubrum*-like propulsion, the more spacious equatorial surface allows for more cilia to be located than in the propulsion strategies of pulled or pushed by cilia covering one end. This might be another reason that much lower flow velocities are generated in the *M. rubrum*-like propulsion.

Although using the ECB for jumping can effectively minimize both the imposed hydrodynamic disturbance and the associated mechanical energy cost, its poor maneuverability can be a disadvantage. This might be the reason that a large group of planktonic protists employ the pulled or pushed strategy for swimming at relatively low speeds.

Stokes' law cannot be used to correctly calculate the swimming/jumping energetics

The instantaneous mechanical power input (Fig. 7c) and total mechanical work (Table 1) calculated from the towed-body CFD model are ~4-23 times smaller than those calculated from the three self-propelled ciliate-jumping models. Using the towed-body model to calculate the jumping energetics in the present CFD study is similar to using the well-known Stokes' law to calculate the energetics. Therefore, using Stokes' law can substantially underestimate the mechanical power input and total mechanical work. The reason for such underestimation is that a dominant percentage of the mechanical energy is dissipated within the ciliary forcing zone (Keller and Wu, 1977), which is, however, not accounted for at all by Stokes' law. Thus, caution has to be taken in interpreting those previous estimates of the energetics for swimming/jumping microorganisms based on Stokes' law. Of importance is the actual morphology involved in the propulsion, as it determines the mechanical energy dissipation within the zones forced by the propulsive morphology and the flow-field pattern outside the forcing zones, both of which affect the overall energetics.

Jump number

Fast jumping by planktonic copepods generates viscous vortex rings (Kiørboe et al., 2010; Jiang and Kiørboe, 2011a; Jiang and Kiørboe, 2011b). Whether or not such vortex rings are generated depends on the impulsiveness of the jump behavior, which can be characterized by a dimensionless

'jump number' (Jiang and Kiørboe, 2011a): $N_{\text{jump}} \equiv \frac{\tau}{d^2/(4\nu)}$, where τ is the duration of the power stroke and d the body length. N_{jump} is the ratio of two time scales (beat duration and viscous time scale). For values of order 1 or less, the generated flow will be in the form of a viscous vortex ring, whereas, for very large values, the generated flow will be in the form of a momentum jet. For ciliate jumping considered in the present study, $N_{\text{jump}} \sim 190$, which is consistent with the CFD simulation results that momentum jets are generated both in front of and behind the ciliate body (Fig. 5).

FUNDING

This work was supported by National Science Foundation grants NSF OCE-0323959 & IOS-0718506 and an award from WHOI's Ocean Life Institute to H.J.

REFERENCES

Bearon, R. N. and Magar, V. (2010) Simple models of the chemical field around swimming plankton. *J. Plankton Res.*, **32**, 1599-1608.

Blake, J. R. (1973) A finite model for ciliated micro-organisms. *J. Biomechanics*, **6**, 133-140.

Blake, J. R. (1971) A spherical envelope approach to ciliary propulsion. *J. Fluid Mech.*, **46**, 199-208.

Brennen, C. (1974) An oscillating-boundary-layer theory for ciliary propulsion. *J. Fluid Mech.*, **65**, 799-824.

Crawford, D. W. (1989) *Mesodinium rubrum*: the phytoplankter that wasn't. *Mar. Ecol. Prog. Ser.*, **58**,161-174.

Darwin, C. (1839) *Journal of researches into the geology and natural history of the various countries visited by H. M. S. Beagle under the command of Captain Fitzroy, R. N. from 1832 to 1836*. Henry Colburn, London.

Fenchel, T. (2001) How dinoflagellates swim. *Protist*, **152**, 329-338.

Fenchel, T. (1987) *Ecology of Protozoa. The Biology of Free-living Phagotrophic Protists*. Science Tech Publishers/Springer-Verlag, Madison.

Fenchel, T. and Finlay, B. J. (1983) Respiration rates in heterotrophic, free-living protozoa. *Microb. Ecol.*, **9**, 99-122.

Fenchel, T. and Hansen, P. J. (2006) Motile behaviour of the bloom-forming ciliate *Mesodinium rubrum*. *Marine Biology Research*, **2**, 33-40.

Gaines, G. and Taylor, F. J. R. (1985) Form and function of the dinoflagellate transverse flagellum. *J. Protozool.*, **32**, 290-296.

Hausmann, K., Hülsmann, N., and Radek, R. (2003) *Protistology*. Schweizerbart'sche Verlagsbuchhandlung, Stuttgart.

Higdon, J. J. L. (1979a) A hydrodynamic analysis of flagellar propulsion. *J. Fluid Mech.*, **90**, 685-711.

Higdon, J. J. L. (1979b) The hydrodynamics of flagellar propulsion: helical waves. *J. Fluid Mech.*, **94**, 331-351.

Hughes, D. E. and Wimpenny, J. W. T. (1969) Oxygen metabolism by microorganisms. In Rose, A. H. and Wilkinson, J. F. (eds.), *Advances in Microbial Physiology*, Vol. 3. Academic Press, New York, pp. 197-231.

Jakobsen, H. H. (2001) Escape response of planktonic protists to fluid mechanical signals. *Mar. Ecol. Prog. Ser.*, **214**, 67-78.

Jiang, H. and Kiørboe, T. (2011a) The fluid dynamics of swimming by jumping in copepods. *Journal of the Royal Society Interface*, doi:10.1098/rsif.2010.0481.

Jiang, H. and Kiørboe, T. (2011b) Propulsion efficiency and imposed flow fields of a copepod jump. *J. Exp. Biol.*, **214**, 476-486.

Jiang, H. and Paffenhöfer, G.-A. (2008) Hydrodynamic signal perception by the copepod *Oithona plumifera*. *Mar. Ecol. Prog. Ser.*, **373**, 37-52.

Jonsson, P. R. and Tiselius, P. (1990) Feeding behaviour, prey detection and capture efficiency of the copepod *Acartia tonsa* feeding on planktonic ciliates. *Mar. Ecol. Prog. Ser.*, **60**, 35-44.

Karp-Boss, L., Boss, E. and Jumars, P. (1996) Nutrient fluxes to planktonic osmotrophs in the presence of fluid motion. *Oceanogr. Mar. Biol.*, **34**, 71-107.

Keller, S. R. and Wu, T. Y. (1977) A porous prolate-spheroidal model for ciliated micro-organisms. *J. Fluid Mech.*, **80**, 259-278.

Kiørboe, T. (1993) Turbulence, phytoplankton cell size, and the structure of pelagic food webs. *Advances in Marine Biology*, **29**, 1-72.

Kiørboe, T., Jiang, H. and Colin, S. P. (2010) Danger of zooplankton feeding: the fluid signal generated by ambush-feeding copepods. *Proc. Roy. Soc. B*, **277**, 3229-3237.

Kiørboe, T. and Visser, A. W. (1999) Predator and prey perception in copepods due to hydromechanical signals. *Mar. Ecol. Prog. Ser.*, **179**, 81-95.

Langlois, V. J., Andersen, A., Bohr, T. et al. (2009) Significance of swimming and feeding currents for nutrient uptake in osmotrophic and interception-feeding flagellates. *Aquat. Microb. Ecol.*, **54**, 35-44.

Lighthill, M. J. (1970) Aquatic animal propulsion of high hydromechanical efficiency. *J. Fluid Mech.*, **44**, 265-301.

Lindholm, T. (1985) *Mesodinium rubrum* - a unique photosynthic ciliate. *Advances in Aquatic Microbiology*, **3**, 1-48.

Magar, V., Goto, T. and Pedley, T. J. (2003) Nutrient uptake by a self-propelled steady squirmer. *Quart. J. Mech. App. Math.*, **56**, 65-91.

Magar, V. and Pedley, T. J. (2005) Average nutrient uptake by a self-propelled unsteady squirmer. *J. Fluid Mech.*, **539**, 93-112.

Margalef, R., Estrada, M. and Blasco, D. (1979) Functional morphology of organisms involved in red tides as adapted to decaying turbulence. In Taylor, D. L. and Seliger, H. H. (eds.), *Toxic Dinoflagellate Blooms*. Elsevier, Amsterdam, pp. 89-94.

Miyasaka, I., Nanba, K., Furuya, K., Nimura, Y. and Azuma, A. (2004) Functional roles of the transverse and longitudinal flagella in the swimming motility of *Prorocentrum minimum* (Dinophyceae). *J. Exp. Biol.*, **207**, 3055-3066.

Munk, W. H. and Riley, G. A. (1952) Absorption of nutrients by aquatic plants. *J. Mar. Res.*, **11**, 215-240.

Packard, T. T., Blasco, D. and Barber, R. T. (1978) *Mesodinium rubrum* in the Baja California upwelling system. In Boje, R. and Tomczak, M. (eds.), *Upwelling Ecosystems*. Springer-Verlag, Berlin, pp. 73-89.

Redfield, A. C. (1958) The biological control of chemical factors in the environment. *American Scientist*, **46**, 205-221.

Reynolds, C. S. (2006) *Ecology of Phytoplankton*. Cambridge University Press, Cambridge.

Riisgård, H. U. and Larsen, P. S. (2009) Ciliary-propelling mechanism, effect of temperature and viscosity on swimming speed, and adaptive significance of 'jumping' in the ciliate *Mesodinium rubrum*. *Marine Biology Research*, **5**, 585-595.

Schmidt-Nielsen, K. (1997) *Animal Physiology: Adaptation and Environment* (Fifth edition). Cambridge University Press, Cambridge.

Sleigh, M. A. (1989) *Protozoa and other protists* (New edition). Edward Arnold, London.

Smith, W. O. and Barber, R. T. (1979) A carbon budget for the autotrophic ciliate *Mesodinium rubrum*. *J. Phycol.*, **15**, 27-33.

Stoecker, D. K., Johnson, M. D., de Vargas, C. and Not, F. (2009) Acquired phototrophy in aquatic protists. *Aquat. Microb. Ecol.*, **57**, 279-310.

Stoecker, D. K., Putt, M., Davis, L. H. and Michaels, A. E. (1991) Photosynthesis in *Mesodinium rubrum*: species-specific measurements and comparison to community rates. *Mar. Ecol. Prog. Ser.*, **73**, 245-252.

Strom, S. L. and Fredrickson, K. A. (2010) Modelling the concentration of exuded dimethylsulphoniopropionate (DMSP) in the boundary layer: reply. *J. Plankton Res.*, **32**, 259–260.

Taylor, F. J. R., Blackbourn, D. J. and Blackbourn, J. (1971) The red-water ciliate *Mesodinium rubrum* and its ''incomplete symbionts'': a review including new ultrastructural observations. *J. Fish. Res. Bd. Canada*, **28**, 391-407.

Tiselius, P., Jonsson, P. R., Kaartvedt, S., Olsen, E. M. and Jorstad, T. (1997) Effects of copepod foraging behavior on predation risk: an experimental study of the predatory copepod *Pareuchaeta norvegica* feeding on *Acartia clausi* and *A. tonsa* (Copepoda). *Limnol. Oceanogr.*, **42**, 164-170.

Visser, A. W., Mariani, P. and Pigolotti, S. (2009) Swimming in turbulence: zooplankton fitness in terms of foraging efficiency and predation risk. *J. Plankton Res.*, **31**, 121-133.

White, F. M. (1974) *Viscous Fluid Flow*. McGraw-Hill, New York.

Wilkerson, F. P. and Grunseich, G. (1990) Formation of blooms by the symbiotic ciliate *Mesodinium rubrum*: the significance of nitrogen uptake. *J. Plankton Res.*, **12**, 973-989.

Wu, T. Y. (1977) Hydrodynamics of swimming at low Reynolds numbers. *Fortschr. Zool.*, **24**, 149-169.

Yih, W., Kim, H. S., Jeong, H. J., Myung, G. and Kim, Y. G. (2004) Ingestion of cryptophyte cells by the marine photosynthetic ciliate Mesodinium rubrum. *Aquat. Microb. Ecol.*, **36**, 165-170.

Appendix: Validation of the CFD code performance

The performance of the unstructured finite-volume CFD software package ANSYS FLUENT (version 12.0.16) has been tested for simulating the low-Reynolds-number flow as well as the associated material transport. Several simple cases involving a body force or an internal solid boundary have been simulated and the results compared against available analytical solutions. Validation of the code performance is a crucial step to establish suitable numerical schemes and parameters for an accurate simulation of the ciliate jumping flow as well as the associated nutrient uptake.

A two-dimensional CFD model for simulating the flow field imposed by a self-propelled infinite half-plane equipped with a ciliary surface layer (Fig. A1) has been shown to be able to reproduce the analytical solution derived by Wu (1977) for this problem (Fig. A2).

Also, excellent code performance has been demonstrated (Fig. A3) for simulating the low-Reynolds-number flow past a stationary solid sphere as well as the associated material transport towards (or away from) the sphere as a sink (or source).

Figure captions

Fig. 1. Schematic drawing of the generalized external morphology of *Mesodinium rubrum* [adapted from Lindholm (1985)]. According to Fenchel and Hansen (2006), the cirri fold to wrap around the oral tentacles at the initiation of a jump, and then the membranelles that form from the cilia of the equatorial ciliary belt (ECB) starts to beat from the aboral end toward the oral end; as a result, the ciliate jumps along the direction indicated by the arrow.

Fig. 2. Kinematics of a typical jump performed by a *Mesodinium rubrum* ciliate. Data are from Fenchel and Hansen (2006). **(a)** Cumulated distance traveled, L, as a function of time, t (after initiation of jump). The fit for L (mm) as a function of t (ms) is: $L = a_3 t^3 + a_2 t^2 + a_{1.5} t^{1.5}$, where $a_3 = 6.118\times10^{-6}$, $a_2 = -6.114\times10^{-4}$ and $a_{1.5} = 4.186\times10^{-3}$, and the fit is only valid for the power-stroke duration (i.e. $0 < t \leq$ 18.6 ms). **(b)** Jumping velocity, U, as a function of t. (c) Body acceleration, A, as a function of t. The slight reversal of the ciliate at the end of the jump was mostly owing to the stretching of the cirri, which was not considered in the present study. Because both the velocity and the distance traveled during the reversal were significantly less than those during the power stroke, the effects due to the reversal on the hydrodynamic signature and nutrient uptake should be minimal.

Fig. 3. Axisymmetric computational fluid dynamics (CFD) model for simulating the flow field imposed by a model ciliate jumping straight rightward. The symmetry boundary condition specifies zero normal velocity and zero normal gradients of all variables at the upper boundary; the pressure-outlet boundary condition specifies a zero static (gauge) pressure at the two side boundaries.

Fig. 4. Illustrations of the four ciliary forcing schemes (see the main text for the details). The meshes in gray immediately surrounding the spherical body mark the ciliary layer on which a spatially distributed, time-dependent body force field, **F**, is applied to model the thrust exerted by ciliary beating.

Fig. 5. Instantaneous flow velocity field imposed by the jumping ciliate at the time instant (~18.6 ms after the initiation of jump) when the ciliate reaches the maximum jump velocity, U_{max} (~10.7 mm s^{-1}),

for **(a)** equatorially distributed cilia; **(b)** anteriorly distributed cilia (pulled); **(c)** posteriorly distributed cilia (pushed); and **(d)** a towed sphere. Plotted in the meridian plane above the axisymmetric axis are contours of flow velocity magnitudes: the grey contour lines show flow velocity magnitudes < U_{max} (minimum = $0.1U_{max}$ with increments of $0.1U_{max}$), the black contours indicate flow velocity magnitudes equal to the instantaneous ciliate jump velocity, U_{max}, and the dotted grey contours indicate flow velocity magnitudes > U_{max} (minimum = $2.0U_{max}$ with increments of U_{max}). Plotted in the meridian plane below the axisymmetric axis are equal-length flow velocity vectors showing flow directions, plotting only vectors with magnitudes > $0.1U_{max}$. For clarity, only a small fraction of the CFD-simulated vectors are shown. A stationary frame of reference is used.

Fig. 6. Time series of volume of influence calculated, respectively, for the four imposed hydrodynamic disturbances. The volume of influence, V, is normalized by the ciliate body volume, $V_{ciliate}$. The threshold velocity, u^*, is 40 μm s^{-1} (a reasonable, yet arbitrary, choice).

Fig. 7. (a) Instantaneous ciliate jump velocity, U (normalized by the maximum jump velocity, U_{max}), as a function of time, t (normalized by the viscous time scale, $t^* = a^2/\nu$). **(b)** Instantaneous thrust, T (normalized by $6\pi\mu a U_{max}$), and **(c)** instantaneous mechanical power input, P (normalized by $6\pi\mu a U_{max}^2$), as functions of t/t^*, calculated, respectively, for the four ciliary forcing schemes.

Fig. 8. Instantaneous chemical concentration field, C/C_∞, around the jumping ciliate at the time instant (~18.6 ms after the initiation of jump) when the ciliate reaches the maximum jump velocity, U_{max} (~10.7 mm s^{-1}), for **(a)** anteriorly distributed cilia (pulled); **(b)** equatorially distributed cilia; **(c)** posteriorly distributed cilia (pushed); and **(d)** a towed sphere. Contours are drawn every 0.05 from 0 (at the ciliate surface) through to 0.95. The chemical diffusivity, D, is 1.0×10^{-9} m^2 s^{-1} (phosphorus diffusivity in water).

Fig. 9. Instantaneous Sherwood number, Sh, as a function of time, t, or the scaled time, t/t_D^* (where $t_D^* = a^2/D$, the diffusion time scale) for the four ciliary forcing schemes (i.e. the four lines labeled respectively by 1, 2, 3, and 4) and also for a theoretical prediction (i.e. the line labeled by 0). The

theoretical prediction is from $\mathrm{Sh}(t) = \{1+[1+\mathrm{Pe}(t)]^{1/3}\}/2$, where $\mathrm{Pe}(t) = 2aU(t)/D$ [modified from the steady state situation considered by Karp-Boss et al. (1996)]. The chemical diffusivity, D, is 1.0×10^{-9} m^2 s^{-1} (phosphorus diffusivity in water).

Fig. 10. *Mesodinium rubrum*-like propulsion (i.e. equatorially distributed cilia). Instantaneous chemical concentration field, C/C_∞, around the jumping model-ciliate at several time instants after the initiation of jump. Contours are drawn every 0.05 from 0 (at the ciliate surface) through to 0.95. The chemical diffusivity, D, is 1.0×10^{-9} m^2 s^{-1} (phosphorus diffusivity in water).

Fig. 11. *Mesodinium rubrum*-like propulsion (i.e. equatorially distributed cilia). CFD-simulated phosphorus-uptake rate, J, as a function of time, t (after initiation of jump), calculated respectively for 3 levels of the external background phosphorus concentration (C_∞ = 0.13, 0.6, 1.43 μmol L^{-1}). The two horizontal dashed lines indicate the likely range of the bloom phosphorus-uptake rates by *M. rubrum* (~0.38×10^{-19}-2.9×10^{-19} mol P μm^{-2} s^{-1}), estimated from a previous field dataset (Packard et al., 1978).

Supplementary data, Fig. A1. Two-dimensional computational fluid dynamics (CFD) model for simulating the flow field imposed by an infinite half-plane equipped with a ciliary surface layer of thickness, l. The half-plane travels leftward at a constant velocity, **U**, as propelled by a continuum distribution of body force, $f_0(y)$, that models the thrusting effect due to the ciliary surface layer. The periodic boundary conditions applied at the left and right boundaries together with the velocity inlet boundary condition applied at the upper boundary approximate an infinite computational domain.

Supplementary data, Fig. A2. Comparison between the CFD result and the analytical solution of Wu (1977). The optimum distribution of the average ciliary continuum force, $f_0(y/l)/f_0^* = 2^{1/2}\sin(\pi y/l)$, under the condition of minimum power required for fixed mean square force, and the corresponding flow velocity profile, $u_0(y/l)/u_0^* = 2^{1/2}\pi^{-2}[\pi y/l + \sin(\pi y/l)]$.

Supplementary data, Fig. A3. (a) Drag coefficient (C_D) for a sphere in the Reynolds number (Re) range of 0.001-10, with comparison among the results obtained using an axisymmetric CFD simulation, the experimental results (White, 1974), the Oseen approximation [$C_D = (24/Re)(1 + 3/16\ Re)$] and the Stokes approximation ($C_D = 24/Re$). $C_D \equiv Drag/(0.5\rho U^2 S_c)$ where S_c is the cross-sectional area of the sphere, and $Re \equiv 2aU/\nu$. **(b)** Sherwood number [Sh; Equation (8)] for a sphere in the Péclet number ($Pe \equiv 2aU/D$) range of 10^{-3}-10^4, with comparison among the CFD results and three theoretical predictions: (1) $Sh = [1+(1+Pe)^{1/3}]/2$ for all Pe in creeping ($Re < 0.1$), uniform flow; (2) $Sh = 0.4957Pe^{1/3}+0.461$; and (3) $Sh = 1+Pe/4+Pe^2\ln(Pe/2)/8$ for $Pe << 1$. The original sources of these equations are provided by Karp-Boss et al. (1996).

Table 1. Summary of the analysis of the simulated jumps with 4 different ciliary forcing schemes.

Ciliary forcing schemes	CFD-simulated total mechanical work for jump (J)	Froude propulsion efficiency	Cost of jumping estimated for the observed jumping period of ~18.6 ms (% total metabolism)	Cost of jumping estimated for a period of 1 s, based on an assumption of 1 s^{-1} jump frequency (% total metabolism)
Equatorially distributed cilia	1.70×10^{-12}	0.775	28	0.53
Anteriorly distributed cilia	1.11×10^{-11}	0.126	185	3.4
Posteriorly distributed cilia	9.07×10^{-12}	0.139	151	2.8
Towed body	4.81×10^{-13}	1.0	8	0.15

The Froude propulsion efficiency is computed based on Equation (6).

Total metabolic rate is determined using an empirically derived cell volume-dependent relationship for growing cultures of heterotrophic protists (Fenchel and Finlay, 1983): $\log_{10}M = 0.75\log_{10}Vol - 4.09$, where M is the total metabolic (respiratory) rate in the units of nL O_2 $cell^{-1}$ hr^{-1}, and Vol is the cell volume in μm^3. In the present case, $Vol = 6.37\times10^3$ μm^3 (for an 11.5 μm radius spherical cell), which gives a respiratory rate of 0.0580 nL O_2 $cell^{-1}$ hr^{-1}. This value is equivalent to a cell volume-specific respiratory rate of 0.113 mol O_2 m^{-3} s^{-1}, which is consistent with data from other sources (e.g. Hughes and Wimpenny, 1969). Based on conventional transformation of 1 liter of O_2 representing 20.1 kJ of work (Schmidt-Nielsen, 1997), the calculated respiratory rate can be converted to a power generation of 3.24×10^{-10} W $cell^{-1}$. This is the value of the total metabolism used here.

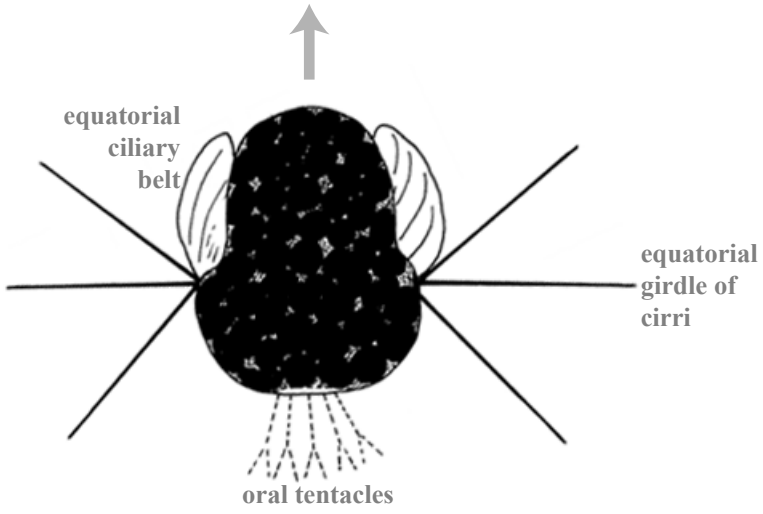
equatorial
ciliary
belt
equatorial
girdle of
cirri
oral tentacles

Figure 1

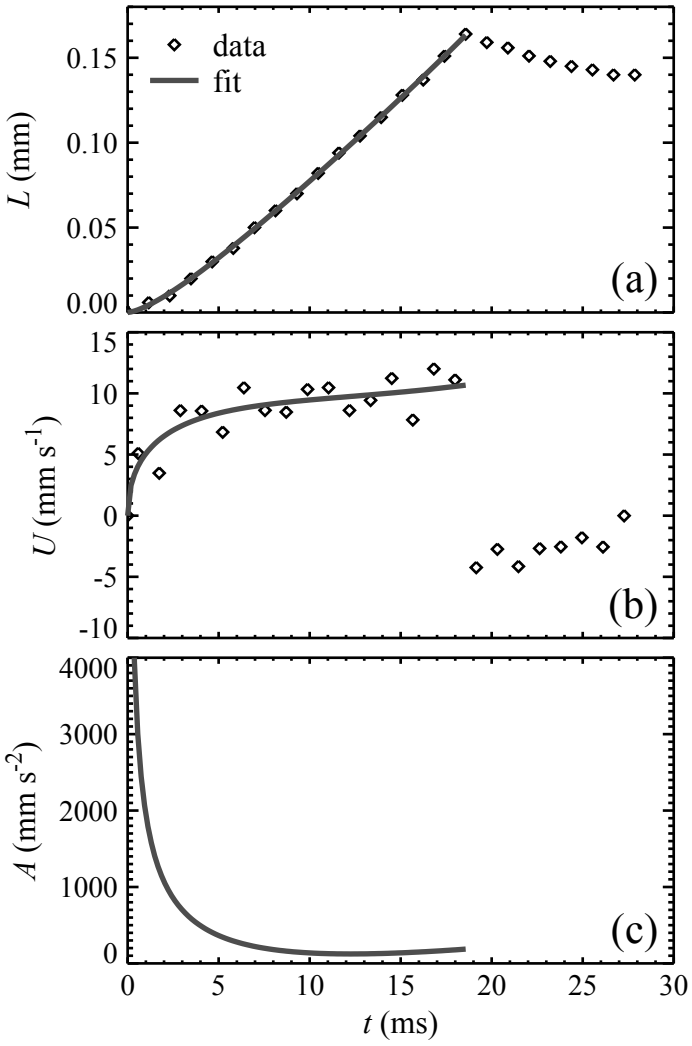
data
fit
L (mm)
0.00
0.05
0.10
0.15
(a)
U (mm s-1)
15
10
5
0
-5
-10
(b)
A (mm s-2)
4000
3000
2000
1000
0
(c)
0
5
10
15
20
25
30
t (ms)

Figure 2

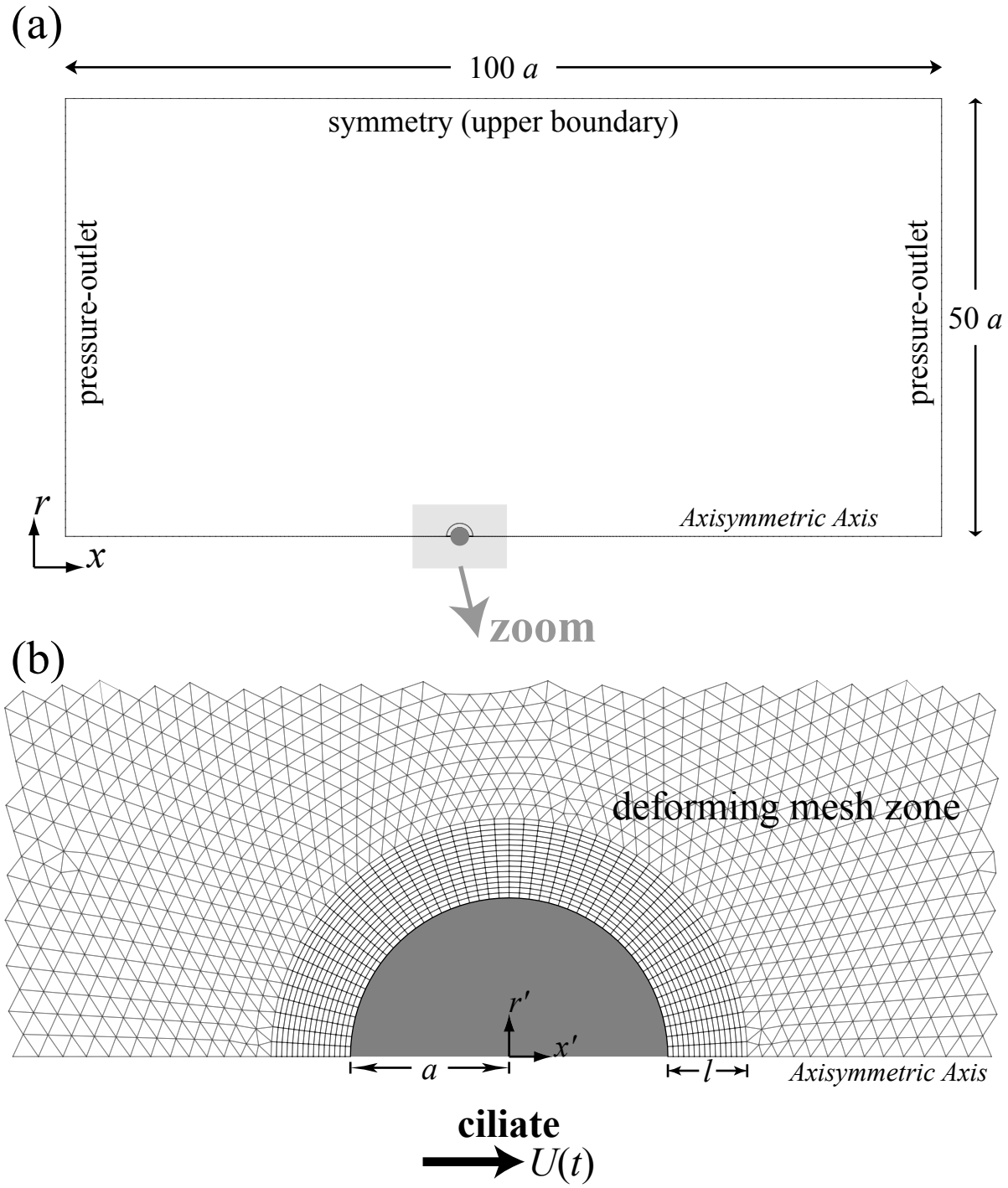
(a)
100 a
symmetry (upper boundary)
pressure-outlet
pressure-outlet
50 a
r
x
Axisymmetric Axis
zoom
(b)
deforming mesh zone
r′
x′
a
l
Axisymmetric Axis
ciliate
U(t)

Figure 3

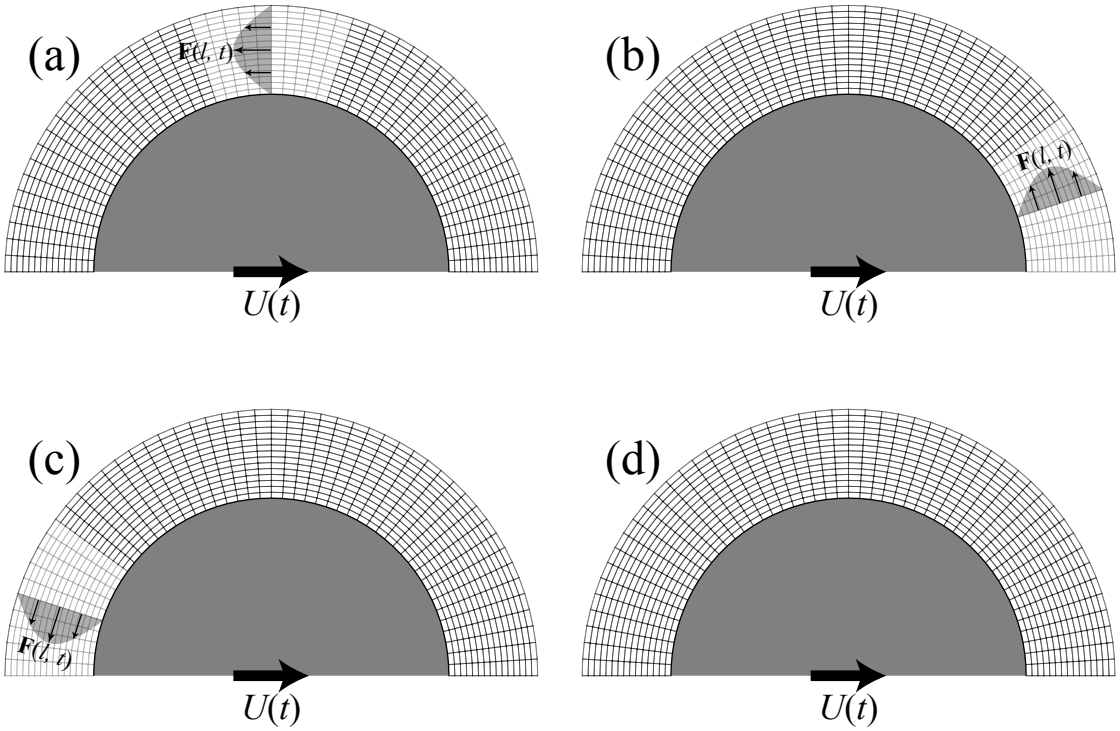

Figure 4

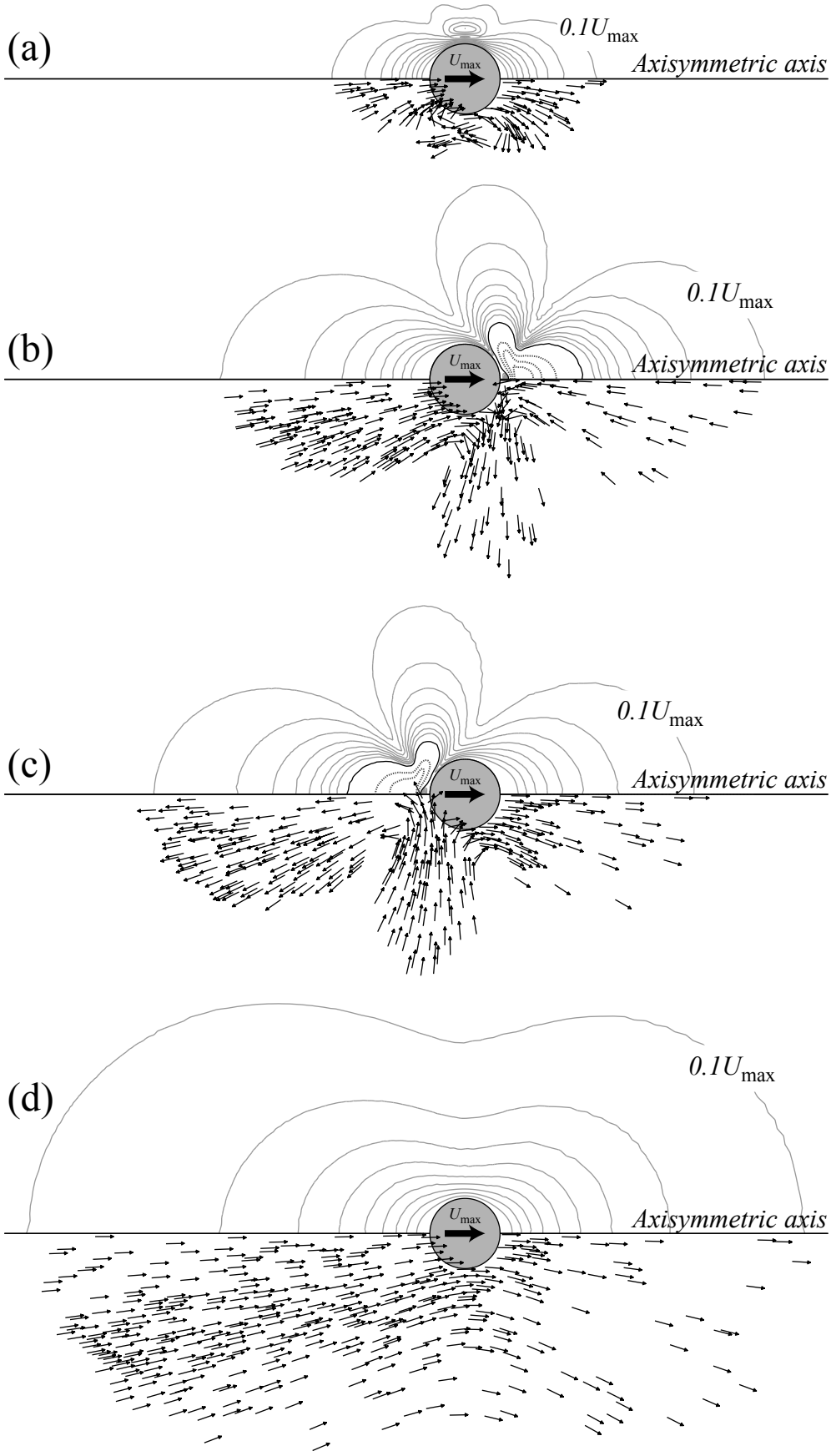
(a)
$0.1U_{max}$
U_{max}
Axisymmetric axis
(b)
$0.1U_{max}$
U_{max}
Axisymmetric axis
(c)
$0.1U_{max}$
U_{max}
Axisymmetric axis
(d)
$0.1U_{max}$
U_{max}
Axisymmetric axis

Figure 5

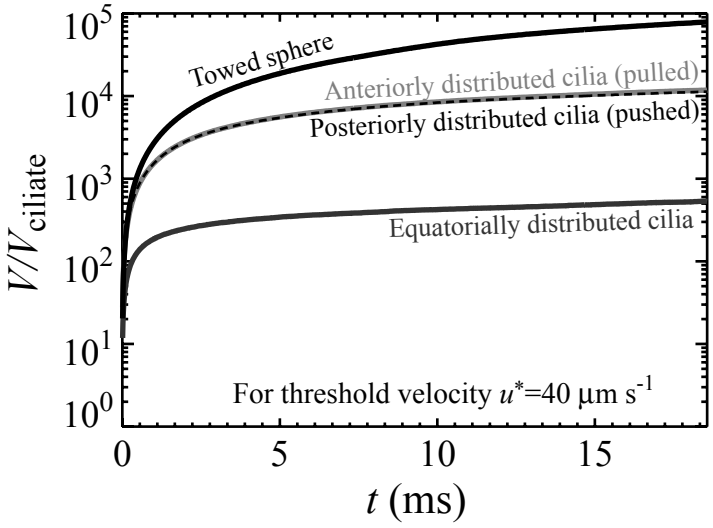
10^5
10^4
10^3
10^2
10^1
10^0
$V/V_{ciliate}$
Towed sphere
Anteriorly distributed cilia (pulled)
Posteriorly distributed cilia (pushed)
Equatorially distributed cilia
For threshold velocity u^*=40 μm s^{-1}
0
5
10
15
t (ms)

Figure 6

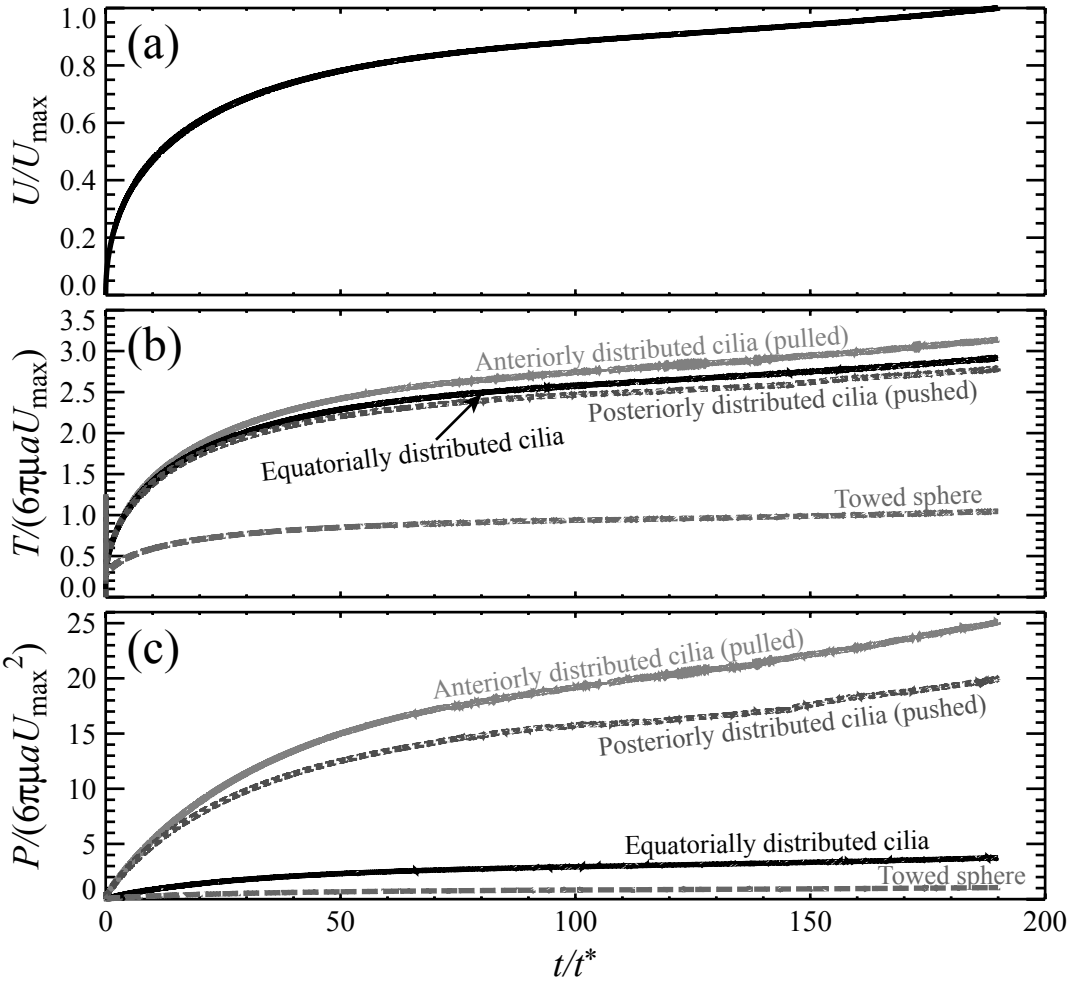
(a)
U/U_{max}
1.0
0.8
0.6
0.4
0.2
0.0
(b)
$T/(6\pi\mu a U_{max})$
3.5
3.0
2.5
2.0
1.5
1.0
0.5
0.0
Anteriorly distributed cilia (pulled)
Posteriorly distributed cilia (pushed)
Equatorially distributed cilia
Towed sphere
(c)
$P/(6\pi\mu a U_{max}^2)$
25
20
15
10
5
0
Anteriorly distributed cilia (pulled)
Posteriorly distributed cilia (pushed)
Equatorially distributed cilia
Towed sphere
0
50
100
150
200
t/t^*

Figure 7

(a) t=18.6 ms: Anteriorly distributed cilia (pulled)

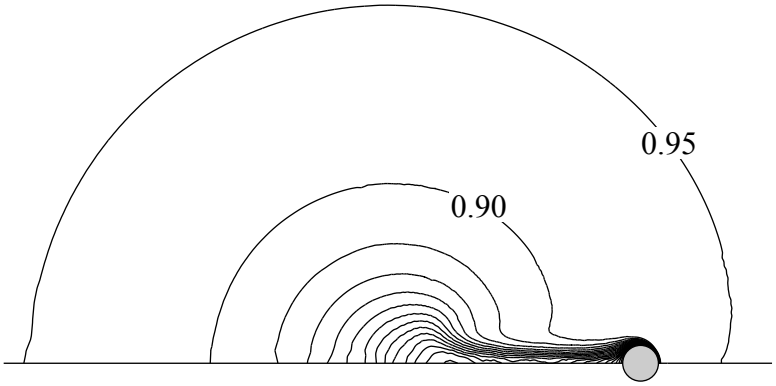

(b) t=18.6 ms: Equatorially distributed cilia

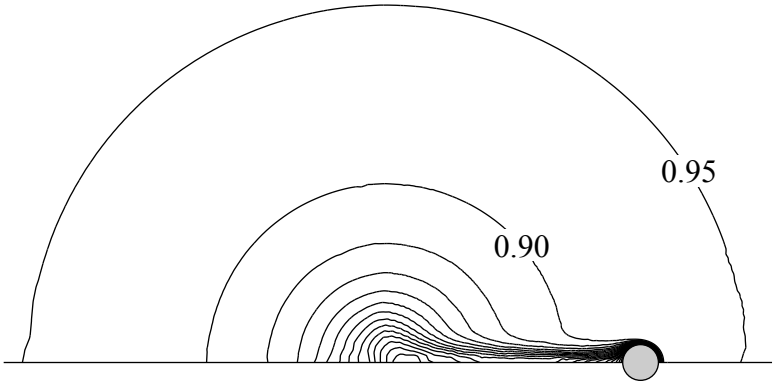

(c) t=18.6 ms: Posteriorly distributed cilia (pushed)

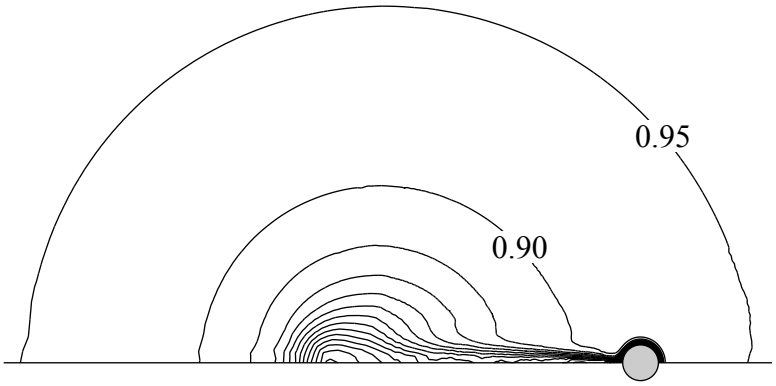

(d) t=18.6 ms: Towed sphere

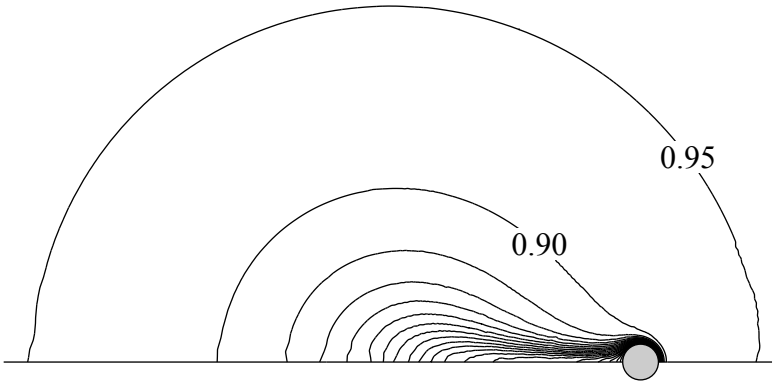

Figure 8

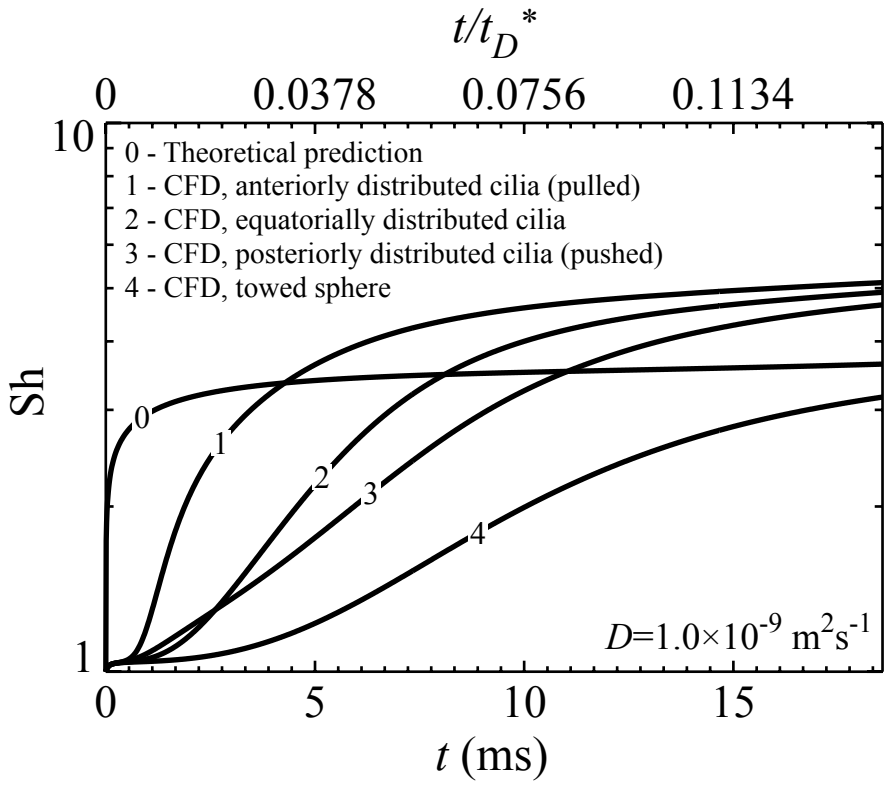
t/t_D^*
0
0.0378
0.0756
0.1134
10
1
Sh
0 - Theoretical prediction
1 - CFD, anteriorly distributed cilia (pulled)
2 - CFD, equatorially distributed cilia
3 - CFD, posteriorly distributed cilia (pushed)
4 - CFD, towed sphere
0
1
2
3
4
D=1.0×10^{-9} m^{2}s^{-1}
0
5
10
15
t (ms)

Figure 9

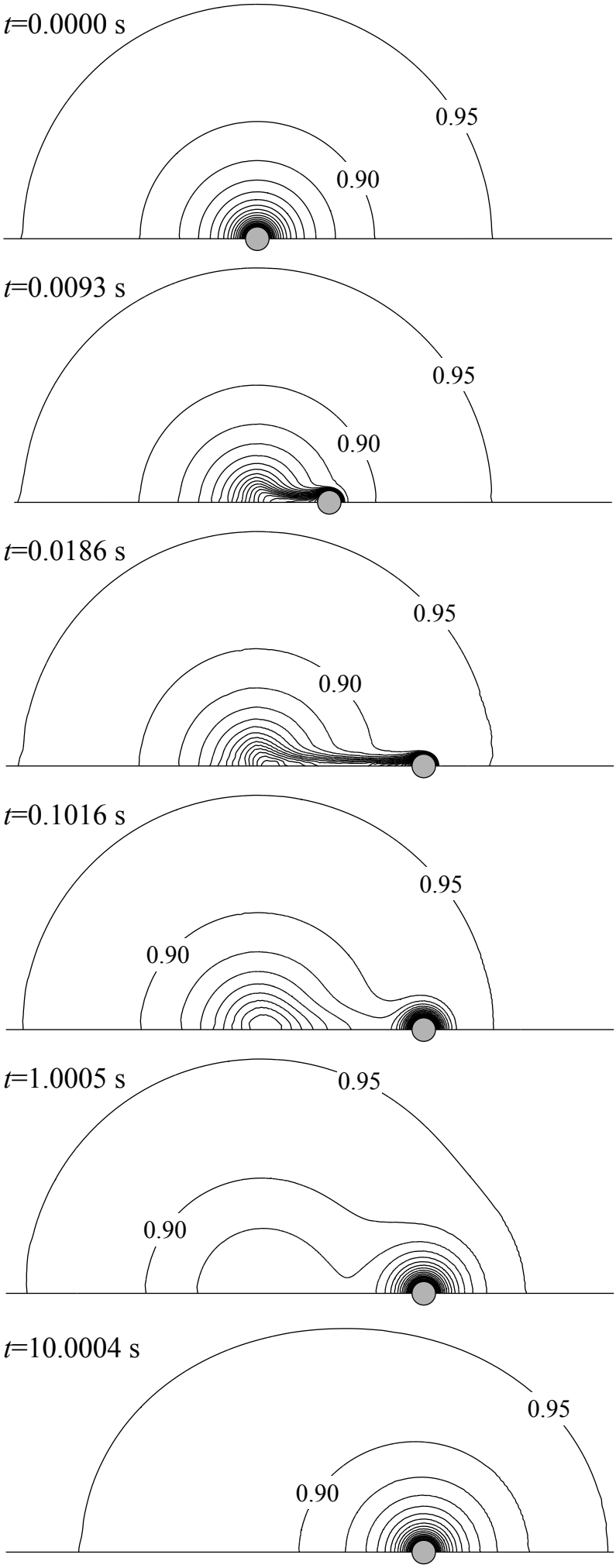
t=0.0000 s
0.95
0.90
t=0.0093 s
0.95
0.90
t=0.0186 s
0.95
0.90
t=0.1016 s
0.95
0.90
t=1.0005 s
0.95
0.90
t=10.0004 s
0.95
0.90

Figure 10

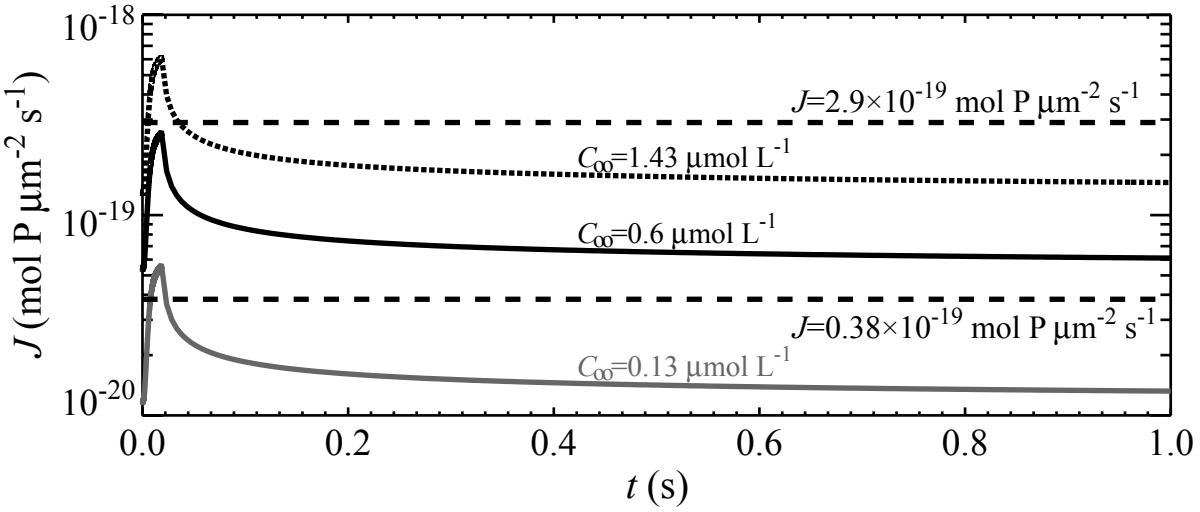
10^{-18}
10^{-19}
10^{-20}
J (mol P µm^{-2} s^{-1})
J=2.9×10^{-19} mol P µm^{-2} s^{-1}
C_∞=1.43 µmol L^{-1}
C_∞=0.6 µmol L^{-1}
J=0.38×10^{-19} mol P µm^{-2} s^{-1}
C_∞=0.13 µmol L^{-1}
0.0
0.2
0.4
0.6
0.8
1.0
t (s)

Figure 11

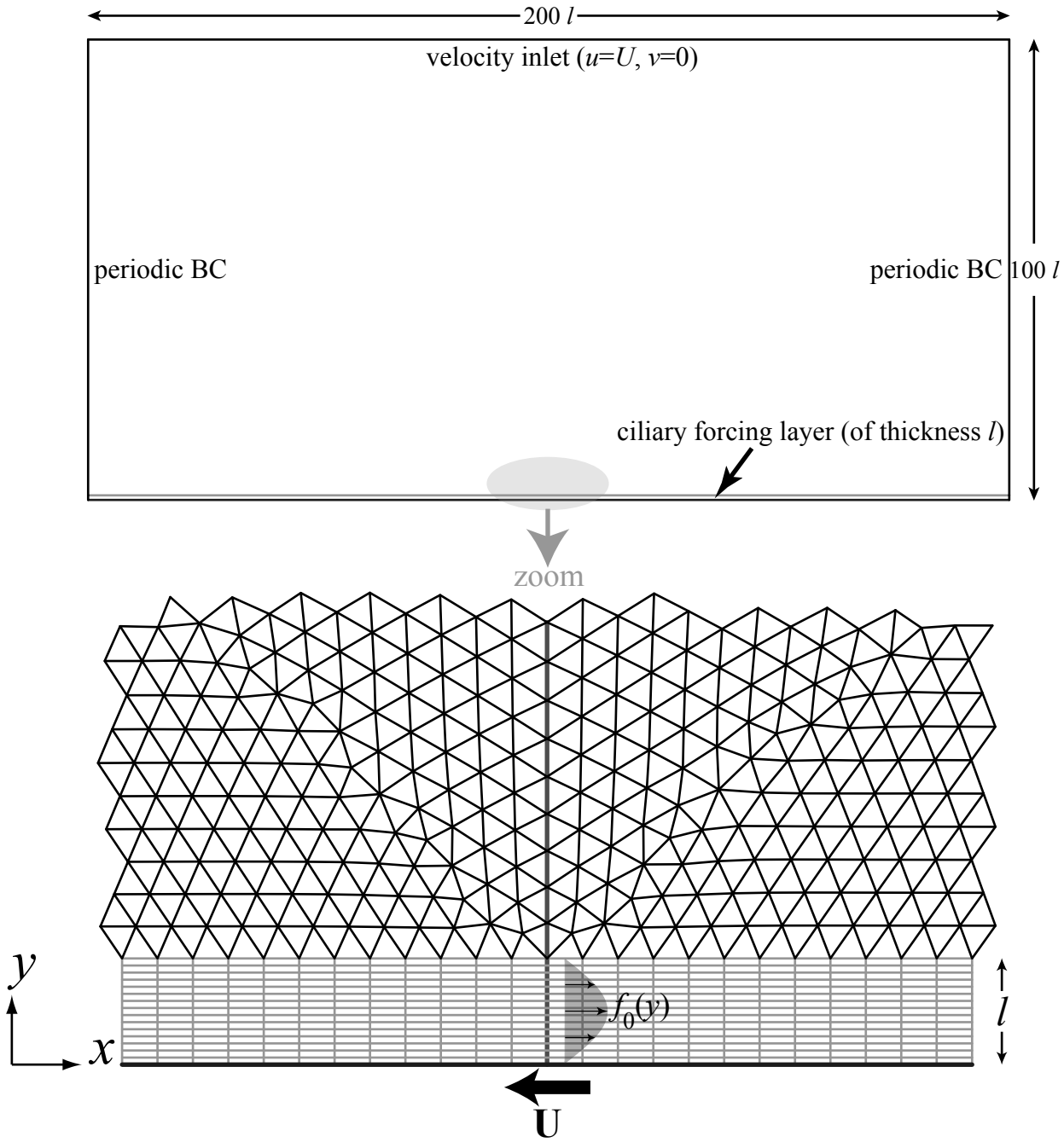
200 l
velocity inlet (u=U, v=0)
periodic BC
periodic BC
100 l
ciliary forcing layer (of thickness l)
zoom
y
x
f0(y)
l
U

Figure A1

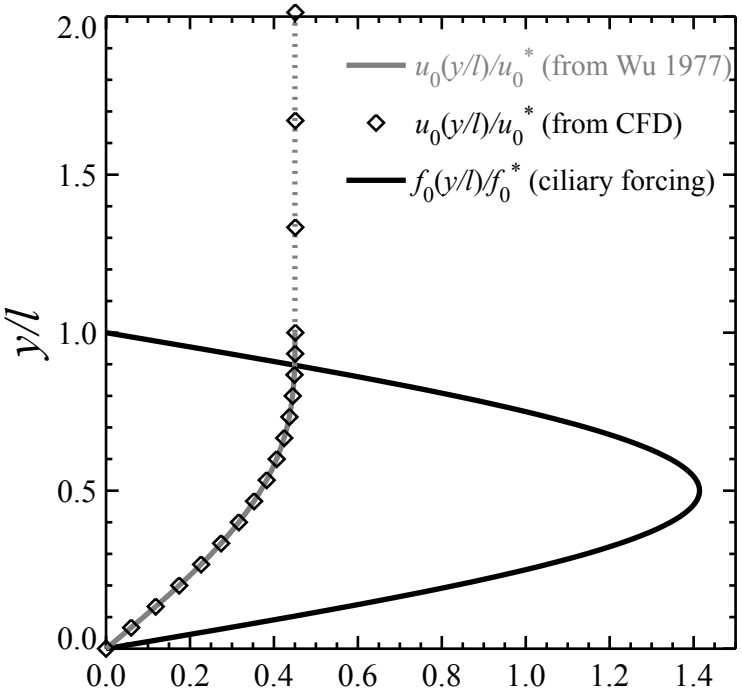
2.0
1.5
1.0
0.5
0.0
y/l
0.0
0.2
0.4
0.6
0.8
1.0
1.2
1.4
u0(y/l)/u0* (from Wu 1977)
u0(y/l)/u0* (from CFD)
f0(y/l)/f0* (ciliary forcing)

Figure A2

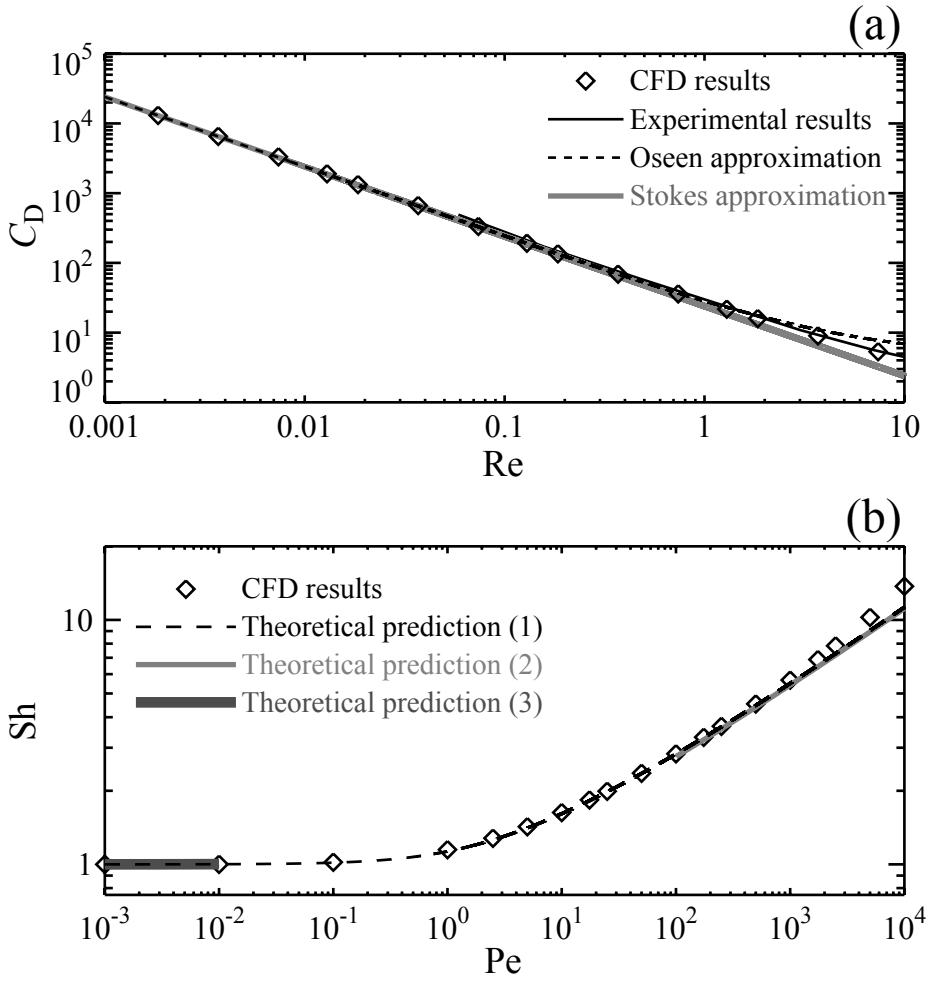
(a)
CFD results
Experimental results
Oseen approximation
Stokes approximation
C_D
Re
(b)
CFD results
Theoretical prediction (1)
Theoretical prediction (2)
Theoretical prediction (3)
Sh
Pe

Figure A3